Advanced Pharmaceutical Bulletin

Accepted Manuscript (unedited)

The manuscript will undergo copyediting, typesetting, and review of the resulting proof before it is published in its final form.

Research Article

How to cite this article:
Morad F, Foroutan T, Shafie S. Application of Electrospun Polycaprolactone/Gelatin/Layered Double Hydroxide/Hymercromone in the Death of Melanoma Cancer Cells. Advanced Pharmaceutical Bulletin, doi: 10.34172/apb.46964

Application of Electrospun Polycaprolactone/Gelatin/Layered Double Hydroxide/Hymercromone in the Death of Melanoma Cancer Cells

Fatemeh Morad[1], Tahereh Foroutan[1*], Seyedeh Sara Shafie[2]

Department of animal sciences, faculty of biological sciences, Kharazmi university, Tehran, Iran
Department of stem cell Stem Cell and Regenerative Medicine Department, Institute of Medical Biotechnology, National Institute of Genetic Engineering & Biotechnology, Tehran, Iran

ARTICLE INFO

Keywords:
PCL,
LDH,
Gelatin,
Coumarin,
Nanofibrous scaffold

Article History:
Submitted: December 20, 2025
Revised: April 11, 2026
Accepted: May 07, 2026
ePublished: May 24, 2026

ABSTRACT

Purpose: The use of drug delivery on nanoparticles has been expanded to improve the efficacy of treatment. The aim of the present study was to investigate the effect of 7 hydroxy 4 methylcoumarin (hymercromone) loaded on synthesized layered double hydroxide (LDH)/polycaprolactone (PCL)/gelatin (Gel) nanofibrous scaffolds on the death of the B16F10 cancer cell line.
Methods: The LDH/hymecromone nanohybrid was prepared using a co-precipitation technique, then incorporated into a PCL/GEL polymer solution and fabricated via electrospuning. The scaffold was characterized in terms of its phase, morphology, and elemental composition using X-ray diffraction, scanning electron microscopy, and energy-dispersive X-ray spectroscopy, respectively. Cell viability was evaluated through the MTT assay, while a Calcein AM/PI dual-staining kit was employed for further analysis using confocal microscopy.
Results: The findings showed that the LDH/hemichromone nanohybrid was properly synthesized and incorporated into the nanofibrous scaffold. It was also found that the addition of LDH nanoparticles to the PCL/Gel scaffold improved its mechanical strength and elongation at break. MTT results revealed that the survival rate of B16F10 cells treated with drug loaded on PCL/Gel/LDH scaffolds for 72 hours was less than 24 hours. Confocal microscopy results also confirmed the MTT results and showed that more cell death occurred at 72 hours than at 24 hours. As the depth of the scaffold approached, the number of cells gradually decreased.
Conclusion: It appears that PCL/Gel/LDH scaffolds can be suitable candidate for drug loading for therapeutic application in cancer cells.

***Corresponding Author**
Tahereh Foroutan, Email: foroutan@khu.ac.ir, ORCID: 0000-0002-1476-3928

Introduction

Melanoma is a malignant skin tumor originating from melanocytes or transformed moles that accounts for 4% of skin cancers and is responsible for more than 80% of skin cancer deaths.[1] Melanoma is one of the most challenging types of skin cancer due to its aggressive behavior, high metastasis rate, multidrug resistance, and high recurrence rate.[2-4] Imbalance between cell proliferation and death caused by damage to apoptotic pathways is considered to be one of the causes of its formation, and restoring these pathways through drugs can be one of the methods of its treatment.[5]

Coumarins, which are secondary metabolites of plants, fungi, and bacteria, have a benzo-α-pyrone structure and exhibit anti-inflammatory, antitumor, and antimelanogenic properties.[6-9] They have significant role in inducing cell death by the regulation of apoptotic molecules and the suppression of anti-apoptotic proteins. [10,11] They inhibit metastasis by inducing the expression of angiogenic factors and matrix metalloproteinases.[12,13] Hymecromone (7-hydroxy-4-methylcoumarin), a coumarin derivative, has attracted much attention due to its antimicrobial, antioxidant, antitumor, antiviral, anti-Alzheimer, and cardio-protective properties.[14] It has shown great potential in overcoming drug resistance, reducing chemotherapy side effects, and improving targeted cancer therapies, and has shown better melanogenic activities than methoxylated coumarins. [15, 16]

In recent years, the development of novel drug delivery systems with the aim of achieving better therapeutic outcomes and fewer side effects has attracted much attention in biomedical research. [17,18] Electrospun nanofibrous scaffolds made of biodegradable polymers offer a suitable platform for drug delivery with a high surface-to-volume ratio, good biocompatibility, and structural similarity to the extracellular matrix.[19, 20] Natural polymers such as gelatin, chitosan, collagen, and silk are ideal candidates for designing biological scaffolds due to their biocompatibility, degradability, and low immunogenicity. [18, 21-23]

However, to overcome limitations such as mechanical weakness, their combination with synthetic polymers such as polycaprolactone (PCL) and PCL -gelatin (PCL/Gel) nanofibrous scaffold can improve mechanical properties and allow for more precise drug control.[24]

It has been reported that the addition of active nanoparticles such as silver, silicates, and graphene to scaffolds, as well as the combination of hydrophilic natural polymers with synthetic polymers, increases their biological performance, structure modification, wettability, and bioavailability.[25-27]Smart drug carriers of layered double hydroxides (LDHs) can play a special role in the design of drug delivery systems. Their structures consisting of divalent and trivalent metal cations offer the possibility of anion exchange and direct loading of anionic drugs into the interlayer galleries. [28-30] High biocompatibility, low cytotoxicity, chemical stability, pH-dependent control, and cost-effective synthesis make LDHs suitable candidates for the design of smart nanofibrous scaffolds. [31, 32]

Incorporation of LDHs into nanofibrous scaffolds protects drug compounds from enzymatic degradation and premature release, improves their bioavailability and cellular uptake, and increases the effectiveness of targeted therapies, especially in combination cancer therapies.[33-35]Thus, the use of LDHs in the synthesis of scaffolds opens up horizons for the treatment of chronic, treatment-resistant diseases such as cancers. The aim of the present study was to investigate the cell death of B16F10 cells cultured on electrospun PCL/Gel nanofibrous scaffolds containing LDH/hymecromone using MTT assay and confocal microscopy. The synthesized scaffolds were characterized using X-ray diffraction (XRD), infrared spectrometer (FTIR), scanning electron microscopy, EDX and tensile tests.

Materials and Methods

Materials

PCL with an average Mn of 70,000–80,000 g·mol^{-1} and Gel were purchased from Sigma. All other chemicals and solvents were obtained from Merck (Darmstadt, Germany). 7-Hydroxy-4-methylcoumarin (hymecromone) was purchased from Sigma-Aldrich.

Preparation and characterization of LDH/ Hymecromone

LDH was synthesized using the coprecipitation method. An aqueous solution of $MgCl_2 \cdot 6H_2O$ (0.6 M) and $AlCl_3 \cdot 6H_2O$ (0.2 M) (3:1 molar ratio) was prepared. Hymecromone solution (0.0003 M) was added dropwise under stirring and nitrogen atmosphere. The pH was adjusted to 10 and stirred overnight at room temperature. The precipitate was centrifuged, washed, and freeze-dried. Characterization was performed using XRD and FTIR. A summary of this method is shown in figure 1A.

Fabrication of Nnanofibrous Scaffolds

PCL and gelatin were dissolved in trifluoroethanol (50:50 wt%) and stirred for 24 h. Electrospuning was performed at 1 mL/h, 15 cm distance, and 17 kV voltage. Aluminum foil was used as collector. Nanofibers were vacuum-dried overnight. A summary of this method is shown in figure 1B.

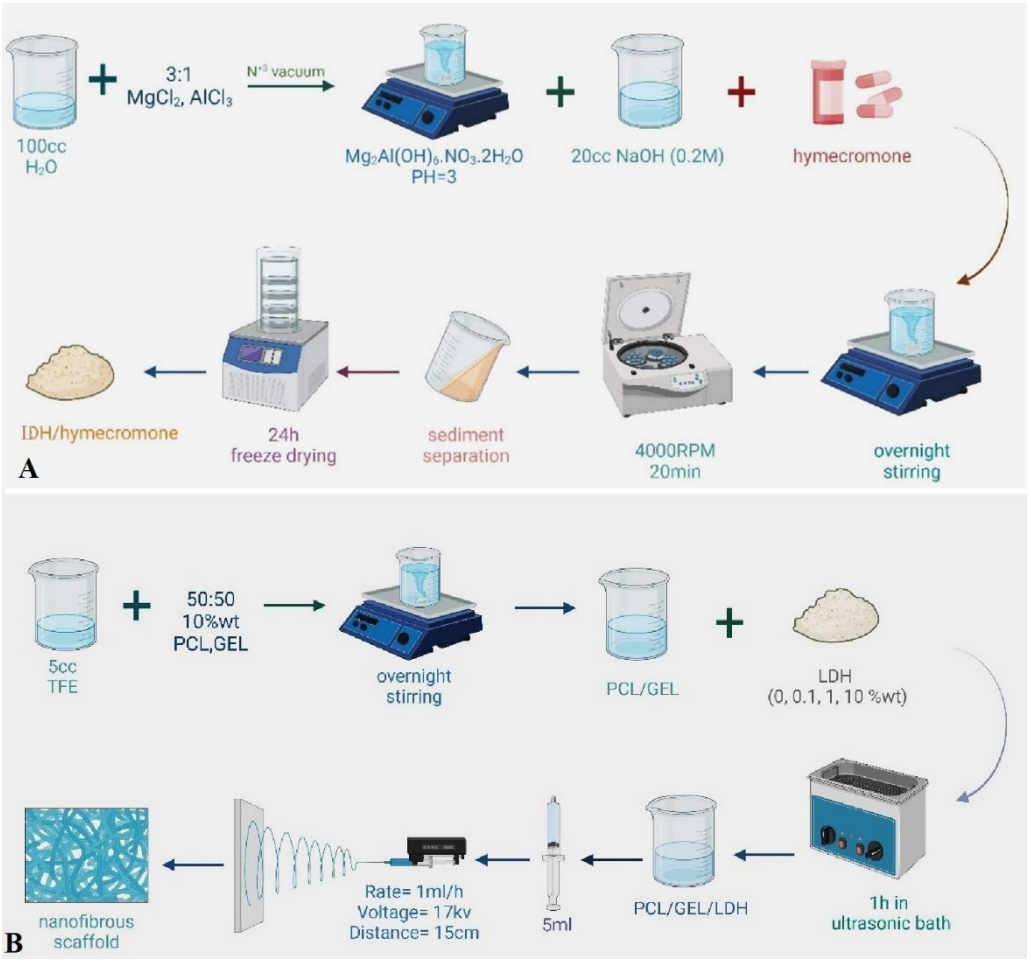

Figure 1. A summary of preparation and characterization of LDH/ Hymecromone (A) and fabrication of nnanofibrous scaffolds (B).

Characterization of scaffolds

SEM was used for morphology analysis (Siemens, D5000-Germany). Samples were gold-coated before imaging. X-ray energy dispersive analysis (EDX) was used for elemental analysis. Fiber diameter was measured using Image J. Mechanical properties were evaluated using a universal testing machine.

Fabrication of PCL/GEL/LDH/Hymecromone Nanofibrous Scaffold

To prepare the electrospun solution, polycaprolactone (PCL) and gelatin (GEL) were dissolved in trifluoroethanol at a weight ratio of 50:50 and stirred continuously for 24 hours. Then, 14 mg of LDH/Hymecromone nanohybrid powder was added to the polymer solution and stirred for 5 minutes to ensure uniform dispersion. The final pH of the solution was measured to be approximately 8. For scaffold fabrication, the prepared solution containing 1 wt% of the nanohybrid was electrospun through a blunt-tip stainless steel needle at a flow rate of 3.5 mL/h utilizing a syringe pump. The space between the needle tip and the collector was set to 10 cm, and an applied voltage of 17 kV was used. Aluminum foil was employed as the collector to gather the nanofibers. Finally, the fabricated nanofibrous scaffolds underwent vacuum drying for a duration of 24 hours to remove any residual solvent. A summary of this method is shown in Diagram 3.

Cell culture study

The mouse melanoma cell line B16F10 obtained from the Pasteur Institute of Iran was cultured in RPMI medium containing 10% FBS (GIBCO, USA), 100 IU/mL penicillin/streptomycin antibiotics (Sigma, USA) at 37°C with 95% humidity and 5% CO2 in air. After passage 3, the cells were cultured on scaffolds of different groups drug PCL/GEL, PCL/GEL/LDH, PCL/GEL/LDH/drug, and drug.

MTT assay

B16F10 cells were divided into 4 groups: control (no treatment), drug (hemochromone), PCL/GEL, PCL/GEL/LDH, and PCL/GEL/LDH/drug and incubated for 48 and 24 hours at 37°C and 5% CO2 atmosphere. MTT (dimethyl thiazole and diphenyltetrazolium bromide) solution (5 mg/mL RPMI) was added to the cells of each group, and after 4 hours, 100 µL dimethyl sulfoxide was added to them to form blue formazan crystals. Then, the optical absorbance of the crystals was measured at a wavelength of 570 nm. A summary of the steps is shown in figure 2A.

Confocal microscopy study

B16F10 cells were cultured on PCL/GEL and PCL/GEL/LDH/drug scaffolds for 24 and 72 hours and double-stained using the Calcein-AM/PI kit (Elabscience, Germany). After washing three times with PBS, the samples were examined by confocal laser microscopy (ZEISS, LSM 800, Germany) at wavelengths of 515 and 617 nm and studied using ZEN BLACK software. A summary of the steps is shown in figure 2B.

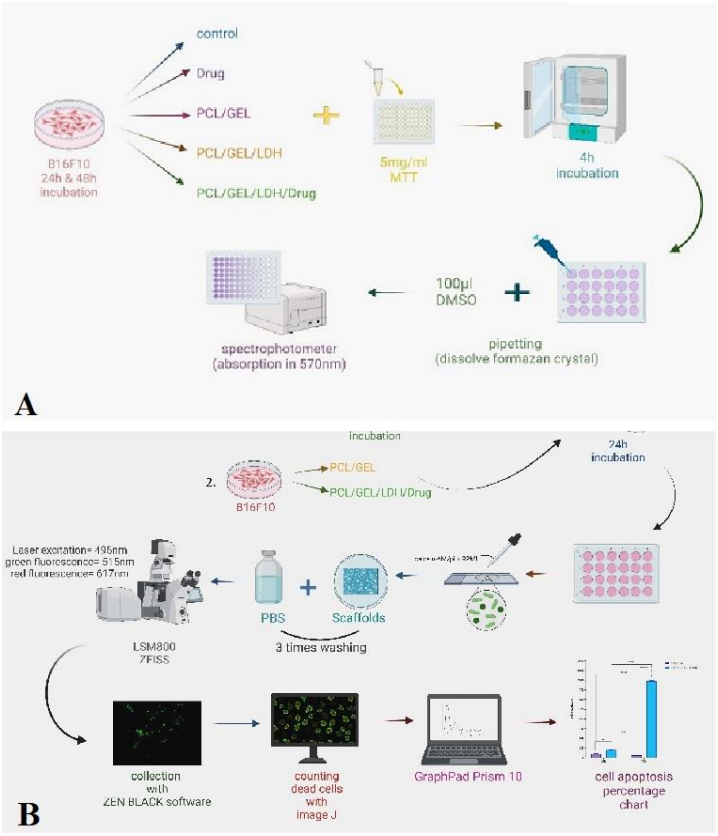

Figure 2. A summary of MMT assay (A) and confocal microscopy study (B) steps.

preparation and characterization of LDH/ Hymecromone (A) and fabrication of nnanofibrous scaffolds (B).

statistical analysis

Data were expressed as mean ± SD. One-way ANOVA was used. $p < 0.05$ was considered significant.

Results

LDH Characterization

LDH nanoparticles were successfully synthesized by the coprecipitation route. The XRD was conducted to identify the presence of crystalline LDH structure and LDH/hymecromone nanohybrids. XRD data of pristine and drug intercalated LDHs are illustrated in figure 3a. As can be seen, the existence of LDH characteristic peaks correspond to the reflections at (003), (006), and (110). This is consistent with the literature. The XRD pattern inferred that the hymecromone is successfully intercalated into LDH. To accommodate the hymecromone molecules, the characteristic peaks are shifted towards lower theta angle because of an increase in the interlayer spacing. Figure 3b shows the SEM micrographs of LDH nanoparticles. The hexagonal platy particles are well separated and form well-defined hexagonal crystals. In contrast, LDH/hymecromone showed agglomeration of nanosheets mainly because of electrostatic interactions between the layers and drug molecules. To investigate the chemical bonds and functional groups present in LDH and LDH/hymecromone samples, infrared spectroscopy (FTIR) analysis was used (figure 3D) (36). The FTIR spectrum confirms the crystallization of LDH by the formation of bonding peaks related to interlayer anions, interlayer water molecules, and O-H bonds related to the layered double hydroxide (table 1).

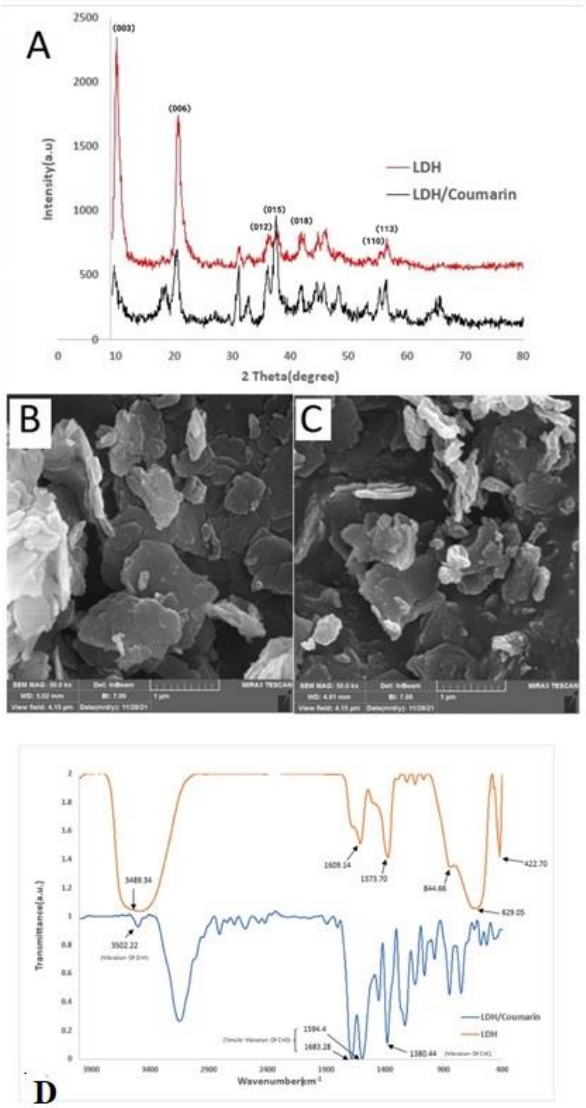

Figure 3. XRD patterns of LDH and LDH/Drug nanocomposite (A). SEM image of mg-Al-LDH (C) LDH/Drug (B). FTIR spectra of LDH and LDH/ hymecromone (D).

Table 1. Three main regions in the FTIR spectrum.

LDH (Cm^{-1})	LDH/hymecromone (Cm^{-1})	Indicate
3489.34	3502.22	OH bond
1373.7	1380.44	NO_3^- ions
1609.14	1594.4	Interlayer water molecules

Electrospun Fiber Characterizations

Figure 4 shows the SEM images of the PCL/Gel/LDH scaffolds. As can be seen, nanofibers are randomly oriented, smooth and bead-free. The mean fiber thickness was estimated by quantified at least 100 fibers using image analysis software, Image J. The average fiber diameter in the pristine PCL/Gel, PCL/Gel/LDH (0.1%), PCL/Gel/LDH (1%), and PCL/Gel/LDH (10%) nanofibers was 0.495, 1.359 µm, 0.492 µm, and 0.729 µm, respectively (Table 2). Overall, adding a slight amount of LDH to the PCL/Gel fibers increased the mean fiber diameter compared to pristine PCL/Gel whereas by increasing the LDH concentration from 0.1% to 1% the mean

fiber diameter declined. As can be seen, upon adding LDH to PCL/Gel, the fiber size distribution is broadened, from several tens of nanometers to a few hundred microns. The widest fiber size distribution was achieved in the PCL/Gel/LDH (1%).

The EDX map of the PCL/Gel/LDH (10%) nanofibers are shown in figure 5. Two peaks correspond to Mg and Al elements in the layered double hydroxide, confirming the uniform distribution of LDH in the PCL/Gel fibers. One peak is related to the nitrogen element in gelatin, and also, carbon and oxygen elements have appeared as two high peaks related to PCL. As seen in figure 5, Magnesium and Aluminum are identified by red and green dots, respectively. Tensile tests were performed on the nanofibers and the results are displayed in figure 6. The representative stress-strain curves demonstrated the sample that has the highest tensile strength was PCL/Gel containing 1 wt % LDH, whereas the PCL/Gel/LDH (10%) showed the lowest tensile strength. The incorporation of LDH nanoparticles into the PCL/Gel nanofibers has increased the ultimate tensile strength. This significant decline in tensile strength in the PCL/Gel/LDH (10%) is caused by the LDHs agglomeration and stress concentration. Also, elongation at break has been improved by adding LDH to PCL/Gel nanofibers. This phenomenon can be attributed to the high surface area and elevated specific stiffness of LDH nanoparticles.

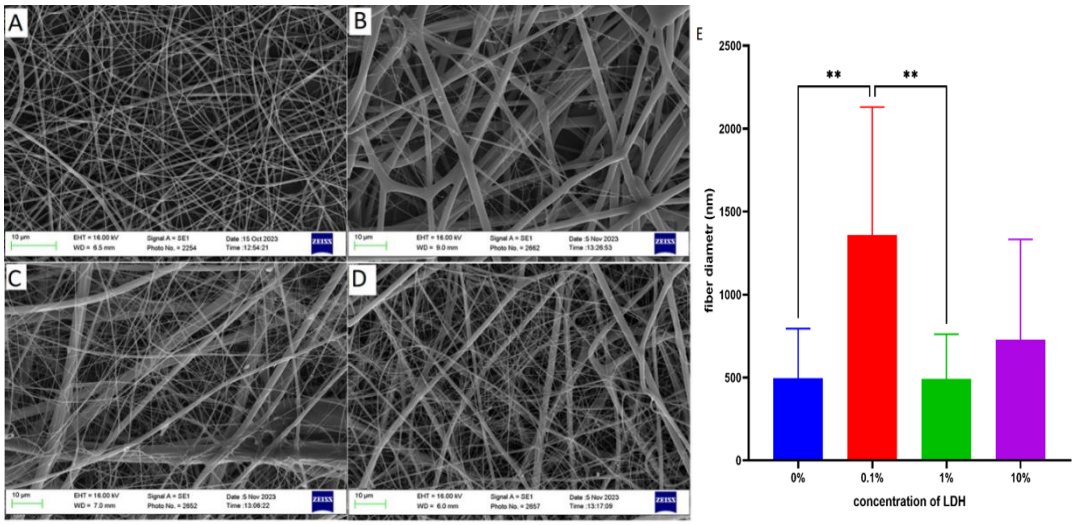

Figure 4. SEM images of PCL/Gel electrospun scaffolds with different percentages of LDH (scale bars represent 10 µm). (A) 0% wt (B) 0.1% wt (C) 1% wt (D) 10 % wt. SEM diagram of fibers diameter average of PCL/Gel scaffolds containing different percentages of LDH (E). p ** < 0.01

Table 2. Average diameter of PCL/ Gel nanofibers containing different percentages of LDH in nanometers.

%LDH	0%	0.1%	1%	10%
Mean	495	1358.9	491.7	728.6
standard deviation	284.6	731.3	255.9	572.2
SD/SEM	1.74	1.86	1.92	1.13

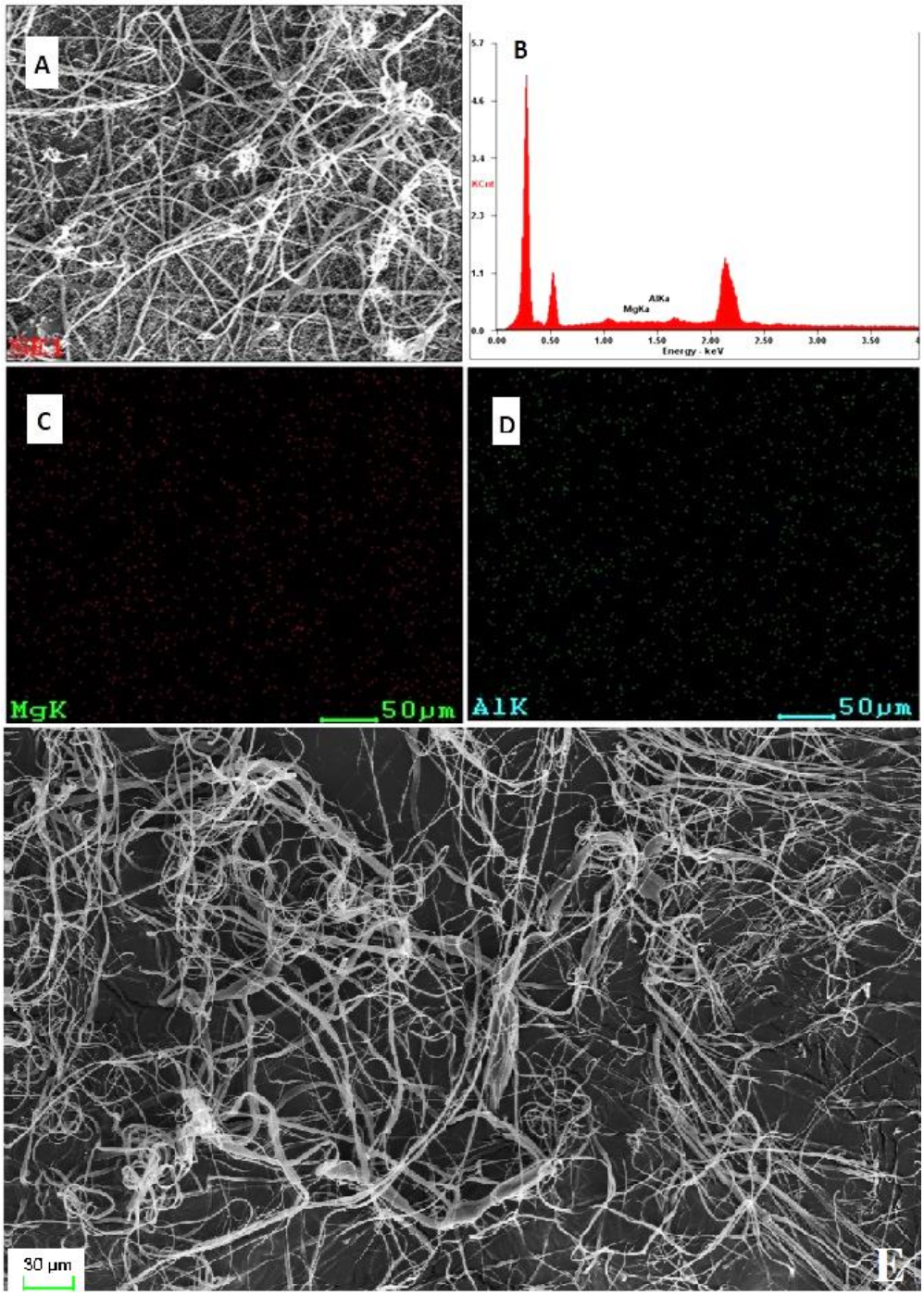

Figure **5.** EDX analysis of PCL/Gel/LDH (10% wt) scaffold shows peaks of carbon, oxygen, nitrogen, Mg and Al (A, B). Elemental mapping analysis for the PCL/Gel/LDH scaffold (Al (blue dots) and Mg (green dots) (C, D). Scanning electron microscopy image of PCL/Gel/LDH/Drug scaffold (E).

.

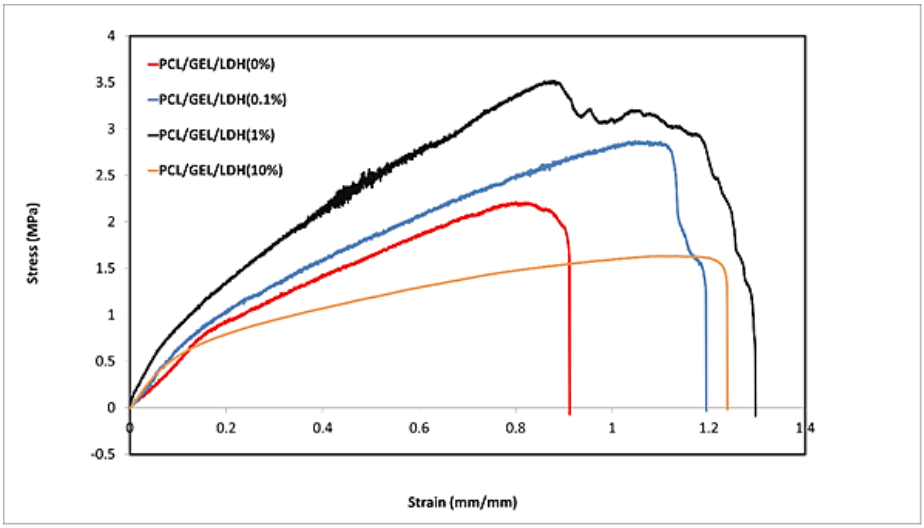

Figure 6. Stress−strain curves of PCL/Gel scaffolds with different percentages of LDH: 0% wt (red), 0.1% wt (blue), 1% wt (black) and 10% wt (yellow)

Cell viability and confocal microscopy Study

The MTT assay was used to assess the survival rate of cultured B16F10 cells on different treatments of PCL/ Gel, PCL/ Gel /LDH, PCL/ Gel /LDH/Drug, and drug alone. figure 7 shows a significant increase in survival rate of B16F10 cells cultured on PCL/ Gel and PCL/ Gel /LDH compared to control group cells after 24h incubation respectively ($P<0.05$, $P<0.01$). The difference between the above groups was more significant after 72 hours of treatment compared to 24 hours ($P<0.01$ and $P<0001$). These results indicate a positive effect of PCL/ Gel and PCL/ Gel /LDH on B16F10 cell survival rates. The results showed that culturing B16F10 cells on scaffold PCL/Gel /LDH/Drug for 24h and 48h significantly reduced their survival rate compared to control group ($P<00001$). The confocal microscopy also confirmed the above results (figure 6, 7). It was observed that cellular drug uptake in the PCL/Gel /LDH/Drug group increased with time. After a longer incubation time (72h), a significant reduction in cell number was observed due to the cytotoxic nature of the drug on B16F10 cancer cells.

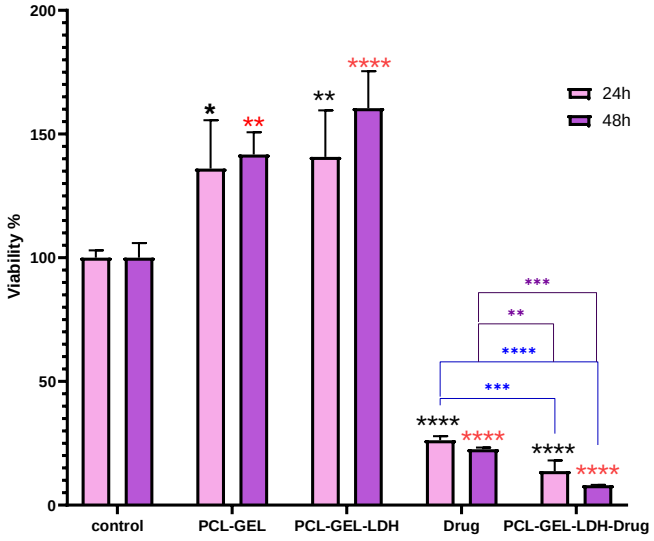

Figure 7. The viability rate of B16F10 cells cultured on different scaffolds after 24 and 48 hours of incubation with MTT test. Asterisks indicate significant differences between control groups and other groups. p * < 0.05, p ** < 0.01, p**** < 0.0001.

Table 3. The average viability of the control group compared to different treatments after 24h and 48h incubation.

Groups	control 24h	control 48h	PCL/Gel 24h	PCL/GEL 48h	PCL/Gel/ LDH 24h	PCL/Gel/ LDH 48h	Drug 24h	Drug 48h	PCL/Gel/ LDH/Drug 24h	PCL/Gel/ LDH/Drug 48h
Mean	100	100	136	141.7	140.8	160.4	26.2	22.6	13.7	**8**
standard deviation	2.4	4.8	15.9	7.3	15.3	12.2	1.3	0.5	3.5	**0.1**

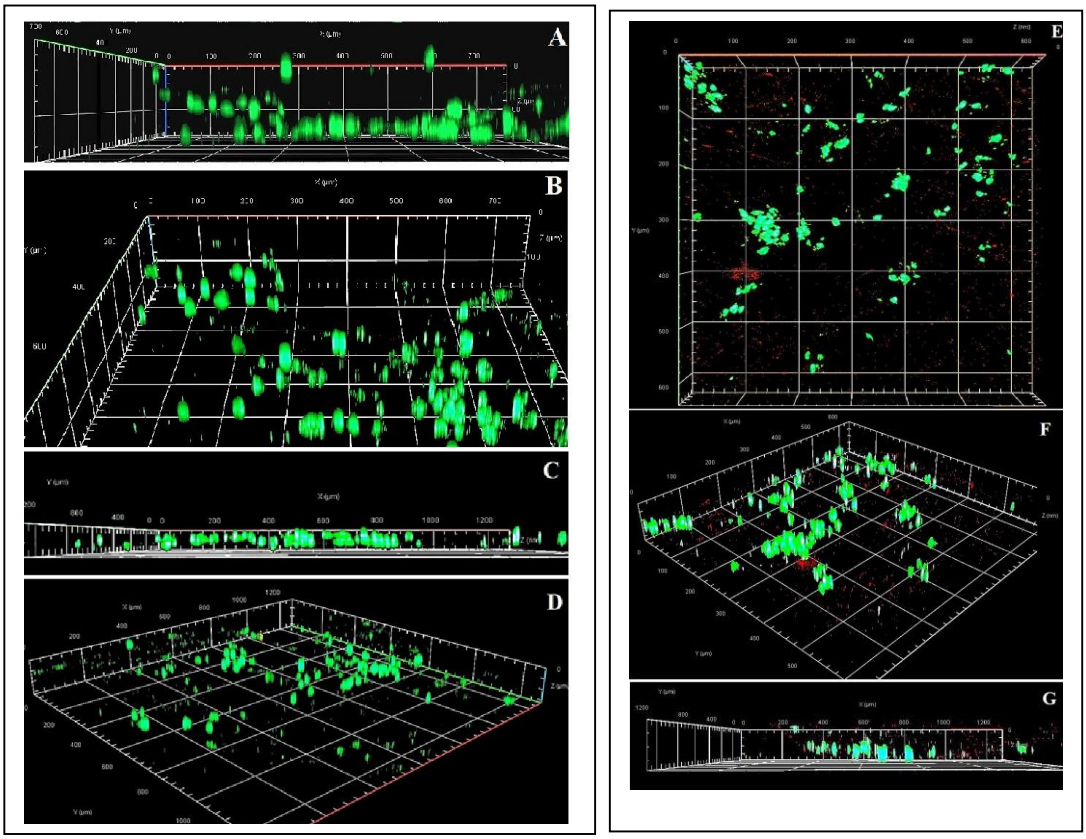

Figure 8. Cellular uptake of drug loaded on PCL/Gel (A, B), PCL/ Gel / LDH (C, D), PCL/ Gel / LDH/Drug (24h) (E) and 72 (F, G) by B16F10 cell line observed by confocal microscopy.

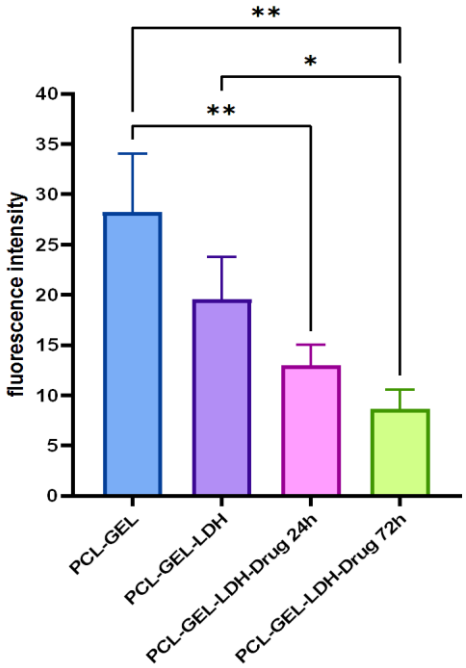

Figure9. Confocal images and green fluorescence intensity

Table 4. green fluorescence intensity obtained from confocal microscopy results.

	PCL-Gel	**PCL-Gel-LDH**	**PCL-Gel-LDH-Drug (24h)**	**PCL-Gel-LDH-Drug (72h)**
mean	28.239	19.543	12.978	8.672
Standard deviation	4.116	2.983	1.438	1.353

Discussion

An ideal drug delivery scaffold should have properties such as biocompatibility, mechanical properties, tunable biodegradability, and sufficient porosity required for drug incorporation. PCL could be a suitable candidate due to its biocompatibility that is easier and faster to degrade.[37, 38]

However, it requires structural modifications due to its hydrophobic nature and very slow degradation.[39] PCL, with its low melting point and excellent biocompatibility with other polymers, is easily compounded and modified. In this study, Gel and LDH nanoparticles were added to increase hydrophilicity, enhance cellular uptake, and enable loading of anionic drugs. We designed a drug delivery system of PCL nanoparticles, Gel, and LDH as carriers for the drug hymecromone, which aimed to deliver the drug to the target cells. XRD and FTIR analyses showed that the drug was successfully encapsulated in the interlayer space of LDH layers. In the XRD spectrum of synthesized LDH, characteristic diffraction peaks were observed at lower 2θ angles (sharp and symmetrical peaks at 11.219° and 22.479°) and higher 2θ angles (broad and asymmetric peaks at 34.513°, 38.38°, 60.266°, 61.452°), corresponding to crystal planes (003), (006), (012), (015), (018), (110), and (113). These patterns indicated a well-ordered layered structure and successful synthesis of LDH via co-precipitation. In the LDH/ hymecromone, shifts in reflections (003) and (006) to lower angles indicated increased interlayer spacing and replacement of nitrate anions with the anionic drug.

FTIR spectra provided complementary evidence. In the LDH sample, distinct bands appeared at 3489.34 cm^{-1} (OH), 1609.14 cm^{-1} (interlayer H_2O), and carbonate ion bands at 844.66, 1373.7, and 629.05 cm^{-1}. Low-energy peaks at 422.7 and 472.07 cm^{-1} were attributed to O–M–O bonds. In the LDH/Drug spectrum, new bands such as 3502.22 cm^{-1} (OH), 1683.28 cm^{-1} (C=O),1594.4, and 1380.46 cm^{-1} (C=C and methyl group) confirmed the presence of hymecromone within the LDH structure.

SEM analysis of the nanocomposite scaffold morphology revealed that adding LDH to PCL/Gel significantly affected fiber diameter. In general, increasing LDH increased the average fiber diameter; however, when LDH increased from 0.1% to 1%, the average fiber diameter decreased to 867 nm. This phenomenon was linked to increased electrical conductivity of the electrospun solution. [40] Solutions with higher conductivity enhance jet charge capacity, producing uniform, bead-free nanofibers with smaller diameters. At 0.1% LDH, conductivity was insufficient, and increased solution viscosity led to larger fiber diameters. EDX elemental analysis confirmed the presence of Mg and Al, indicating uniform LDH dispersion on the fiber surface.

In terms of mechanical properties, the scaffold containing 1% LDH showed the highest tensile strength, which was attributed to the reduction in fiber diameter, increased crystallinity, and olecular orientation.[41] Overall, the

addition of LDH increases the mechanical properties of the scaffold compared to the original samples, which is essential for maintaining structural integrity until the drug reaches the target cells.

Biocompatibility and anticancer efficacy evaluations of PCL/Gel/LDH containing hemichromone yielded remarkable results. MTT assay showed that the PCL/Gel scaffold was not only nontoxic to B16F10 cells but also increased cell viability by 41.72%. Furthermore, the use of hemichromone together with LDH nanohybrid in the nanofibrous scaffold significantly reduced cancer cell viability. While the use of the free drug caused a 75.6% decrease in cell viability compare to the control group, the drug-loaded PCL/Gel/LDH scaffold led to a 89.15% reduction. It could be interpreted that the incorporation of LDHs into nanofibrous scaffolds protects drug compounds from enzymatic degradation and premature release, increases bioavailability, improves cellular uptake, and enhances the efficacy of targeted therapies, especially in combination cancer therapies. [34, 35] Furthermore, this superior performance is attributed to the anion exchange structure of LDH, which allows for direct loading of anionic drugs and maintains sufficient positive charge to facilitate cellular uptake despite a relative reduction in surface charge. [42-44] The cationic framework of LDH also protects drugs from enzymatic degradation and enables slower release, reducing side effects and increasing drug stability. LDH layers provide a hydrophilic microenvironment for anionic drugs and act as "molecular containers" for sustained drug release. [31, 45-47] Therefore, after 48 hours of incubation compared to 24 hours, cell viability of B16F10 cells cultured on PCL/Gel/LDH/Drug scaffolds decreased further.

Confocal microscopy images confirmed the results of the MTT assay. In the PCL/Gel/LDH/Drug group, the number of viable cells decreased as the depth of the scaffold approached (figure 8, 9) (Table 4). While in the PCL/Gel group, not only was there no decrease in cell number, but an increase in cell number was observed as the depth of the scaffold approached. The results imply that the positive charge of LDH and its ability to penetrate cell membranes is the main obstacle to the effective transport of the drug into the cytoplasm.[48, 49] The findings demonstrate that integrating LDH/hymecromone into the PCL/Gel scaffold not only improves mechanical and biocompatibility properties but also enhances its anticancer performance in a 3D cell culture model. These results align with previous studies on localized drug delivery and highlight the high therapeutic potential of this system.

Conclusion

In the present research, electrospun PCL/Gel/LDH/ hymecromone scaffolds were developed as a novel drug system for cancer cell death. The combination of polycaprolactone with gelatin enhanced the scaffold's hydrophilicity and biodegradability, while the incorporation of LDH nanoparticles improved mechanical characteristics, including tensile strength and break elongation. SEM imaging and tensile testing revealed that the scaffold containing LDH exhibited optimal mechanical performance and was selected for subsequent cellular studies. The results demonstrated that the PCL/Gel/LDH scaffold was biocompatible and non-toxic to B16F10 cells, even promoting cell viability. The successful incorporation of LDH/hemichromone nanohybrids into the scaffold facilitated cellular drug uptake due to the cationic nature of LDH and enhanced drug stability. These features resulted in increased apoptosis in B16F10 melanoma cells after 48 and 72 h of incubation compared to 24 h. The present hybrid nanofibrous system appears to show great potential as a biodegradable and effective platform for topical anticancer drug applications.

Authors' Contribution

Conceptualization: Tahereh Foroutan, Fatemeh Morad

Data curation: Tahereh Foroutan, Seyedeh Sara Shafiei
Formal analysis: Fatemeh Morad
Investigation: Fatemeh Morad
Methodology: Tahereh Foroutan, Seyedeh Sara Shafiei
Project adoradministration: Tahereh Foroutan,
Resources: Fatemeh Morad
Software: Fatemeh Morad
Supervision: Tahereh Foroutan, Seyedeh Sara Shafiei
Validation: Fatemeh Morad
Writing–original draft: Fatemeh Morad
Writing–review & editing: Tahereh Foroutan

Competing Interests

The authors report there are no competing interests to declare.

Ethical Approval

Kharazmi University, Tehran, Iran (Ethical approval number: IR.KHU. REC.1403.115)

References

1. Mattia G, Puglisi R, Ascione B, Malorni W, Carè A, Matarrese P. Cell death-based treatments of melanoma:conventional treatments and new therapeutic strategies. *Cell Death Disease* 2018; 9(2): 112. doi:10.1038/s41419-017-0059-7

2. Barriera-Silvestrini P, Iacullo J, Knackstedt TJ. American joint committee on cancer staging and other platforms to assess prognosis and risk. *Clin Plast Surg 2021;* 48(4): 599–606. doi: 10.1016/j.cps.2021.05.004

3. Saeidi Z, Giti R, Rostami M. Mohammadi F. Nanotechnology-based drug delivery systems in the transdermal treatment of melanoma. *Adv Pharm Bull 2023*. 13(4): 646–662. doi: 10.34172/apb.2023.070

4. Rabik CA, Dolan ME. Molecular mechanisms of resistance and toxicity associated with platinating agents. *Cancer Treat Rev 2007*; 33(1):9–23. doi: 10.1016/j.ctrv.2006.09.006

5. Bauer J.H, Helfand SL. New tricks of an old molecule: lifespan regulation by p53. Aging Cell 2006; 5(5): 437–40. doi: 10.1111/j.1474-9726.2006.00228.

6. Szliszka E, Czuba ZP, Domino M, Mazur B, Zydowicz G, et al. Ethanolic extract of propolis (EEP) enhances the apoptosis- inducing potential of TRAIL in cancer cells. *Molecules 2009*; 14(2): 738–54. doi.org/10.3390/molecules14020738

7. Sunagawa Y, Kawaguchi S, Miyazaki Y, Katanasaka Y, Funamoto M, Shimizu S, et al. Auraptene, a citrus peel-derived natural product, prevents myocardial infarction-iduced heart failure by activating PPARα in rats. *Phytomed 2022;* 107: 154457. doi: 10.1016/j.phymed.2022.154457

8. Kim T, Hyun CG. Imperatorin positively regulates melanogenesis through signaling pathways involving PKA/CREB, ERK, AKT, and GSK3β/β-catenin. *Molecules 2022;* 27. doi: 10.3390/molecules27196512. doi.org/10.3390/molecules27196512

9. Lee Y, Hyun CG. Mechanistic insights into the ameliorating effect of melanogenesis of psoralen derivatives in B16F10 melanoma cells. *Molecules 2022;* 27. doi: 10.3390/molecules27092613. doi: 10.3390/molecules27092613

10. Sabt A, Abdelhafez OM, El-Haggar RS , Madkour HMF, Eldehna WM, et al. Novel coumarin-6-sulfonamides as apoptotic anti-proliferative agents: synthesis, in vitro biological evaluation, and QSAR studies. *J Enzyme Inhib Med Chem 2018;* 33(1): 1095–1107. doi: 10.1080/14756366.2018.1477137

11. Chuang JY, Huang YF, Lu HF, Ho HC, Yang JS, Li TM, et al. Coumarin induces cell cycle arrest and apoptosis in human cervical cancer heLa cells through a mitochondria- and caspase-3 dependent mechanism and NF-κB down-regulation. *In Vivo 2007;* 21(6): 1003.

12. Kimura Y, Sumiyoshi M. Antitumor and antimetastatic actions of dihydroxycoumarins (esculetin or fraxetin) through the inhibition of M2 macrophage differentiation in tumor-associated macrophages and/or G1 arrest in tumor cells. *European Journal of Pharmacology 2015;* 746: 115–125. doi: 10.1016/j.ejphar.2014.10.048

13. Lee S, Sivakumar K, Shin WS, Xie F, Wang Q. Synthesis and anti-angiogenesis activity of coumarin derivatives. *Bioorg Med Chem Lett 2006; 16(17): 4596–4599.* doi: 10.1016/j.bmcl.2006.06.007

14. Mustafa YF. Aldabbagh N.Th. N, Biological potentials of hymecromone-based derivatives: A systematic review. *Systematic Review Pharmacy 2020; 11: 438–452*. doi:10.31838/srp.2020.11.65

15. Aldabbagh N Th, Mustafa YF. Anticancer properties of hymecromone-derived compounds: A review. *Int J Pharm Res 2020; 13:2163–2174.* doi:10.31838/ijpr/2021.13.01.347

16. Kim T, Kim KB, Hyun CG. A 7-Hydroxy 4-Methylcoumarin Enhances Melanogenesis in B16-F10 Melanoma Cells. *Molecules 2023; 28,* DOI: 10.3390/molecules28073039. doi: 10.3390/molecules28073039

17. Mitchell M.J, BillingsleY MM, Haley RM, Wechsler ME, Peppas NA, Langer R. Engineering precision nanoparticles for drug delivery. *Nat Rev Drug Discov 2021; 20(2): 101–124.* doi: 10.1038/s41573-020-0090-8

18. Reddy, K.T.K. and A.S. Reddy, Recent breakthroughs in drug delivery systems for targeted cancer therapy: an overview. *Cell Mol Biomed Rep 2025; 5(1): p. 13–27.*

19. Mpekris F, Voutouri C , Panagi M , Baish JW, Jain RK, Stylianopoulos T. Normalizing tumor microenvironment with nanomedicine and metronomic therapy to improve immunotherapy. *J Cont Rel 2022; 345: p. 190–199.* doi: 10.1016/j.jconrel.2022.03.008

20. Chandra J, Hasan N, Nasir N, Wahab S, Thanikachalam PV, Sahebkar A, et al. Nanotechnology-empowered strategies in treatment of skin cancer. *Environ Res 2023; 235: p. 116649*. doi: 10.1016/j.envres.2023.116649

21. Suri K, Pfeifer L, Cvet D, Li A, McCoy M, et al. Oral delivery of stabilized lipid nanoparticles for nucleic acid therapeutics. *Drug Deliv Transl Res 2024.* doi: 10.1007/s13346-024-01709-4

22. Xu R, Fang Y, Zhang Z, Cao Y, Yan Y, Gan L, et al. Recent advances in biodegradable and biocompatible synthetic polymers used in skin wound healing. *Materials 2023; 16: p. 5459.* doi: 10.3390/ma16155459

23. Mohite P, Pouri A, Munde S, Dave R, Khan S, Patil R, et al. Potential of chitosan/gelatin-based nanofibers in delivering drugs for the management of varied complications: A review. *Polymers 2025; 17: 435.* doi.org/10.3390/polym17040435

24. Wan Y, Lu X, Dalai S, Zhang J. Thermophysical properties of polycaprolactone/chitosan blend membranes. *Thermochimica Acta, 2009. 487(1): p. 33–38.* doi.org/10.1016/j.tca.2009.01.007

25. Foroutan T, Kabiri F, Motamedi E. Silica magnetic graphene oxide improves the effects of stem cell-conditioned medium on acute liver failure. *ACs omega 2021*; 6 (33). doi: 10.1021/acsomega.0c05395

26. Özder MN, Yelkenci A, Kucak M, Altinbay A, Ustundag CB, Ciftci F. Development and characterization of a polycaprolactone/graphene oxide scaffold for meniscus cartilage regeneration using 3D bioprinting. *Pharm* 2025; 17: 346. doi.org/10.3390/pharmaceutics17030346

27. Yao L, Yuan L, Guo X, Jiang N, Li X, Zhao Q. Curcumin biosynthesized silver nanoparticles-loaded polycaprolactone nanofibers for antibacterial applications. *Mate Technol 2025; 40.* doi.org/10.1080/10667857.2024.2445641

28. Foroutan T, Kassaee MZ, Salari M, Ahmady F, Molavi F. Moayer F. Magnetic Fe3O4@graphene oxide improves the therapeutic effects of embryonic stem cells on acute liver damag. *Cell Prol 2021; e13126: 1*-13. doi.org/10.1111/cpr.13126.

29. Ladewig K, Xu Z, Lu M. Layered double hydroxide nanoparticles in gene and drug delivery. *Expert opin drug deliv 2009; 6: 907–22.* doi: 10.1517/17425240903130585

30. Jin W, Lee D, Jeon Y, Park DH. Biocompatible hydrotalcite nanohybrids for medical functions. *Minerals 2020; 10: 172.* doi.org/10.3390/min10020172

31. Lv F, Xu L, Zhang Y, Meng Z. Layered double hydroxide assemblies with controllable drug loading capacity and release behavior as well as stabilized layer-by-layer polymer multilayers. *ACS Appl Mater Interfaces 2015*; 7(34): 19104–19111. doi.org/10.1021/acsami.5b04569

32. Senapati S, Thakur R, Verma SP, Duggal S, Mishra DP, Das P, et. al. Layered double hydroxides as effective carrier for anticancer drugs and tailoring of release rate through interlayer anions. *J Cont Rel 2016; 224:186–198.* doi: 10.1016/j.jconrel.2016.01.016

33 Tabish M, Yasin G, Anjum MJ, Malik MU, Zhao J, Yng Q, et al. Reviewing the current status of layered double hydroxide-based smart nanocontainers for corrosion inhibiting applications. *J Mat Res Technol 2021; 10: 390–421.* doi.org/10.1016/j.jmrt.2020.12.025

34. Ameena Shirin V.K , Sankar R, Johnson AP, Gangadharappa HV, Pramod K. Advanced drug delivery applications of layered double hydroxide. *J Cont Rel 2021; 330: 398–426.* doi.org/10.1016/j.jconrel.2020.12.041

35. Derusova DA, Vavilov VP. Druzhinin NV, Shpil'noi VY, Pestryakov AN. Detecting defects in composite polymers by using 3D scanning laser doppler vibrometry. *Materials 2022; 15.* doi: 10.3390/ma15207176

36. Mirzavand M, Foroutan T, Hedayati S, Shavandi M, Eslami H, Shafiei SS. Development of electrospun nanofibers containing layered double hydroxide/coumarin nanohybrid for potential wound healing. *J Biomed Mater Res Part B: Appl Biomat 2026;* 114: e70032. doi.org/10.1002/jbmb.70032

37. Khandwekar A.P, Patil DP, Shouche Y, Doble M. Surface engineering of polycaprolactone by biomacromolecules and their blood compatibility. *J Biomat Appl 2010; 26(2): 227–252.* doi: 10.1177/0885328210367442

38. Dhanaraju MD, Gopinath D, Ahmed MR, Jayakumar R, Vamsadhara C. Characterization of polymeric poly(ϵ-caprolactone) injectable implant delivery system for the controlled delivery of contraceptive steroids. *J Biomed Mat Res Part A 2006; 76(1): 63–72.* doi: 10.1002/jbm.a.30458

39. Hajiali F, Tajbakhsh S, Shojaei A. Fabrication and properties of polycaprolactone composites ontaining calcium phosphate-based ceramics and bioactive glasses in bone tissue engineering: A review. *Polymer Review* 2017; 58. doi: 10.1080/15583724.2017.1332640

40. Ahmadi S, Shafiei SS, Sabouni F. Electrospun nanofibrous scaffolds of polycaprolactone/gelatin reinforced with layered double hydroxide nanoclay for nerve tissue engineering applications. *ACS Omega 2022*; 7(32): 28351–28360. doi: 10.1021/acsomega.2c02863

41. Wong S.C, Baji A, Leng S. Effect of fiber diameter on tensile properties of electrospun poly(ε-caprolactone). *Polymer 2008;* 49(21): 4713–4722. doi.org/10.1016/j.polymer.2008.08.022

42. Xu ZP, Zeng QH, Lu GQ , Yu AB. Inorganic nanoparticles as carriers for efficient cellular delivery. *Chem Engin Sci 2006*; 61: p. 1027–1040. doi.org/10.1016/j.ces.2005.06.019

43. Kriven WM, Kwak SY, Wallig MA, Choy JH. Bio-resorbable nanoceramics for gene and drug delivery. *Mat Res Soc* 2004; 29: 33–37. doi.org/10.1557/mrs2004.14

44. Xu ZP, Niebert M, Porazik K, Walker TL, Coope HM, Middelberg AP, et al. Subcellular compartment targeting of layered double hydroxide nanoparticles. *J cont Rel* 2008; 130: 86–94. doi: 10.1016/j.jconrel.2008.05.021

45. Wang H, Wang H, Zou Q, Boerman OC, Nijhuis AWG, Li Y, et al. Combined delivery of BMP-2 and bFGF from nanostructured colloidal gelatin gels and its effect on bone regeneration in vivo. *J Cont Rel 2013; 166.* doi: 10.1016/j.jconrel.2012.12.015

46. Kim YH, Furuya H, Tabata Y. Enhancement of bone regeneration by dual release of a macrophage recruitment agent and platelet-rich plasma from gelatin hydrogels. *Biomatials 2014; 35(1): 214–224.* doi: 10.1016/j.biomaterials.2013.09.103

47. Sun H, Zhang H, Evans DG, Duan X. Synthesis and characterization of nanoscale magnetic drug-inorganic composites. C*hinese Sci Bull 2005; 50(8): 752–757.* doi.org/10.1007/BF03183673

48. Li S, Zhang W, Xue H, Xing R, Yan X. Tumor microenvironment-oriented adaptive nanodrugs based on peptide self-assembly. *Chem Sci 2020;* 11, 8644. doi.org/10.1039/D0SC02937H

49. Zheng M, Tao W, Zou Y, Farokhzad OC, Shi B. Nanotechnology-based strategies for siRNA brain delivery for disease therapy. *Trends Biotechnol 2018; 36(5):562-575.* doi: 10.1016/j.tibtech.2018.01.006